



Injection Properties According to the Inner Shape of Metal Additive Layer Manufactured Coaxial Injectors

J. Ahn¹, K. Ahn^{1†} and H. Y. Lim²

¹ School of Mechanical Engineering, Chungbuk National University, Chungbuk, 28644, Republic of Korea

² Launcher Propulsion Control Team, Korea Aerospace Research Institute, Daejeon, 34133, Republic of Korea

†Corresponding Author Email: kbahn@cbnu.ac.kr

(Received December 14, 2021; accepted April 11, 2022)

ABSTRACT

The application of three-dimensional (3D) printing technology in rocket engine development has numerous benefits considering cost and time. Among the various techniques of 3D printing, the selective laser melting method has the advantage of being able to manufacture complex structures and process multiple materials. In this study, five types of coaxial injectors with different internal configurations were manufactured using metal 3D printing. To confirm the atomization and mixing performance according to the structure of each injector's oxidizer and fuel post, a cold flow test using water and air was performed under a wide range of experimental conditions. As a result of analyzing the injection pressure drop, discharge coefficient, spray pattern, breakup length, and spray angle, the shape of the oxidizer post had a significant influence on the performance of the injector. In comparison, the effect of the fuel post structure was relatively small; however, there was a meaningful difference in the breakup length and spray angle depending on the direction of rotation.

Keywords: 3D printing; Cold flow test; Shear coaxial injector; Swirl coaxial injector; Spray characteristics.

NOMENCLATURE

A_g	nozzle exit passage area of the fuel injector	\dot{m}_l	liquid mass flow rate through the oxidizer injector
A_h	oxidizer inlet hole area	\dot{m}_{ld}	nominal liquid mass flow rate
A_o	nozzle exit area of the oxidizer injector	n	number of oxidizer inlet holes
Cd_g	discharge coefficient of the fuel injector	P_{atm}	atmospheric pressure
Cd_l	discharge coefficient of the oxidizer injector	P_g	gas injection pressure
d_F	nozzle exit diameter of the fuel injector	R	radial distance from the injector center to the center of the oxidizer inlet hole
d_o	nozzle exit diameter of the oxidizer injector	t_o	oxidizer post tip thickness
D_h	hub diameter of the swirler in the fuel injector	V_g	gas axial velocity in the fuel injector exit
D_t	tip diameter of the swirler in the fuel injector	V_l	liquid axial velocity in the oxidizer injector exit
h_l	liquid film thickness in the oxidizer injector exit	2α	full taper angle of the oxidizer injector nozzle
J	gas-to-liquid momentum flux ratio	β	swirler angle
K	swirl injector geometric constant	γ	specific heat ratio
L_B	breakup length	ΔP_l	liquid injection pressure drop through the oxidizer injector
L_R	recess length	θ_s	spray angle
\dot{m}_g	gas mass flow rate through the fuel injector	μ	liquid viscosity
\dot{m}_{gd}	nominal gas mass flow rate	ρ_g	gas density
		ρ_l	liquid density

1. INTRODUCTION

The limitations of many aspects of space launch vehicle development are the cost and time required to design and manufacture various parts. Among the various components, an injector is responsible for the atomization and mixing of the propellant in the combustor and significantly impacts rocket engine performance. Since injectors have diverse and complex structures depending on propellant types and operating conditions, it requires a considerable amount of time to develop a new injector. Several aerospace research institutes and companies are attempting to introduce 3D printing technology to reduce the cost and time resources of space launch vehicle development. Starting with the production of parts with a simple structure, research on the development of engine parts that require complex and precise processing, such as turbine blades and injectors, is currently ongoing (Soller *et al.* 2015, 2016, 2017; Terracciano *et al.* 2017; Lim and Roh 2019; Atyam and Sojka 2017). Illustratively, the Space X's Merlin engine is equipped with an oxidizer valve printed with a 3D printer, and the Relativity Space's Terran 1 aims to manufacture and apply most parts through 3D printing (Howell 2014; Relativity Space 2020). Additionally, the Korea Aerospace Research Institute successfully conducted the combustion test of a 1-ton methane engine combustor built with a 3D printer (Lee *et al.* 2020).

Recent studies present actively conducted research and development of methane engines owing to the demand for reusable and economical launch vehicles. Our research team manufactured an injector using a 3D printer's selective laser melting (SLM) technology with the goal of developing a methane engine with a 3-ton thrust. The SLM technology utilizes a high-power, high-density laser to selectively melt the metal powder and has the advantage of using various materials and forming complex structures (Yap *et al.* 2015). For an engine using liquid oxygen and liquid methane, the injector was set as a coaxial type in which an oxidizer injector and a fuel injector were coaxially combined, and injectors with various internal structures were designed based on the advantages of the SLM method.

Generally, the liquid/gas coaxial injectors consist of an internal liquid oxidizer injector and an external gaseous fuel injector (Huzel and Huang 1992). The liquid oxidizer is supplied to the injector through the oxidizer inlet, and the shape of the inlet determines the type of the injector, either the shear coaxial type or the swirl coaxial type. In the shear coaxial injector, the liquid oxidizer is mostly sprayed with only the axial velocity, whereas in the swirl coaxial injector, the oxidizer inlet is tangentially machined, providing both axial and tangential velocities to the oxidizer (Glogowski and Micci 1995; Cohn *et al.* 2003). Therefore, the two injectors inject the oxidizer in different spray forms under the same flow conditions, resulting in different propellant atomization and mixing performances. Moreover, the resulting spray may

have a different spraying form when the shape of the fuel injector also has a swirl form.

The research team manufactured oxidizer injectors and fuel injectors in various designs through SLM layering in this study and examined how these designs affect the spray characteristics of coaxial injectors. First, we looked at the injection pressure drop and discharge coefficients, which are fundamental requirements for injectors. Next, we measured the breakup length (L_B) and spray angle (θ_s) to determine atomization and mixing performances, utilizing instantaneous images and average images via image processing analysis.

2. EXPERIMENTAL METHODS

2.1 Injectors

The injector was fabricated via SLM layering using UNS S31603 metal powder. The surface roughness and tolerances of the manufactured injectors were Ra 13 μm and $\pm 50 \mu\text{m}$. In the case of the targeted expander cycle methane engine, injectors supply gaseous methane and liquid oxygen. Therefore, a coaxial injector widely used in the liquid/gas propellant combination was designed, and its schematic diagram is shown in Fig. 1.

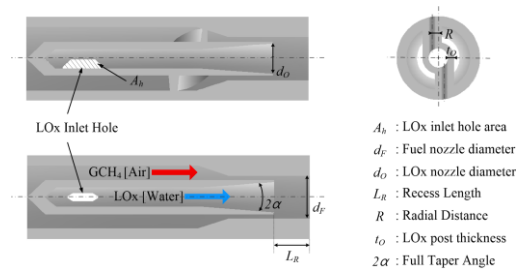


Fig. 1. Cross-section of coaxial injectors (top: swirl coaxial and bottom: shear coaxial).

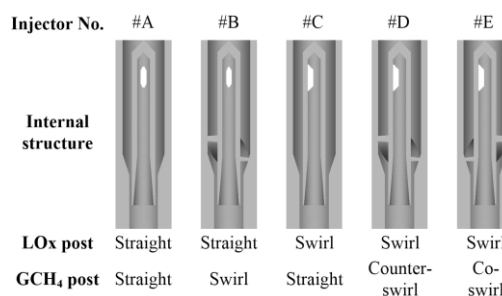


Fig. 2. Internal configuration of each coaxial injector.

Liquid oxygen is supplied from the oxidizer manifold through the oxidizer inlet inside the injector, and gaseous methane is injected from the fuel manifold through the inlet at the top of the injector. To inspect the difference because of the shape of each oxidizer/fuel injector, five types of injectors with different designs were fabricated. Fig. 2 shows the cross-sectional view of each injector, representing their characteristics.

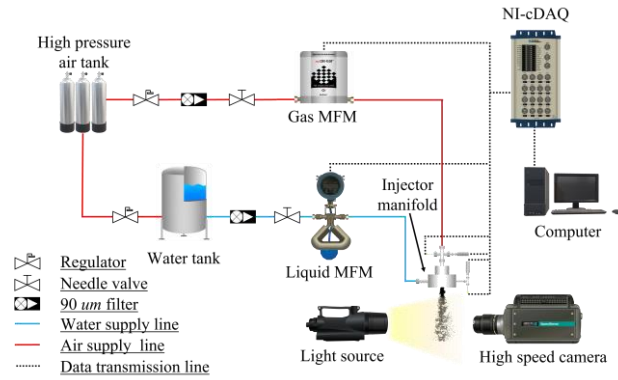


Fig. 3. Schematic diagram of the experimental set-up.

Inj #A and #B were manufactured in a non-swirl type in which the oxidizer inlet is located at the center of the injector, where the liquid oxidizer is supplied into the injector with primarily axial velocity and some radial velocity. However, in the case of Inj #B, a swirler-shaped passage was additionally layered, so gaseous fuel swirls while being injected. In the case of Inj #C, #D, and #E, where the oxidizer inlet is fabricated tangential to the center of the injector, the liquid oxidizer is supplied into the injector and sprayed with both axial and tangential velocity. The swirl injector geometric constant (K) is calculated using Eq. (1), and the swirl injector used in this study has a K value of 0.6 (Ahn and Choi 2017).

$$K = \frac{2A_O R}{nA_h d_O} \quad (1)$$

Moreover, the shape of each fuel injector determines whether gaseous fuel is injected with only the axial velocity, or with rotation in the same or opposite direction to that of the liquid oxidizer. The injector with the swirler-shaped fuel passage was designed to have a rotation angle of 42° in all injectors. The swirl number (SN) can be calculated using Eq. (2), proposed by Beer and Chigier (1972). The #B, #D, and #E swirlers used in this experiment had a hub diameter (D_h) of 6 mm, an inner diameter (D_i) of 10 mm, and the calculated SN gave 0.74.

$$SN = \frac{2}{3} \left[\frac{1 - (D_h / D_i)^3}{1 - (D_h / D_i)^2} \right] \tan \beta \quad (2)$$

The oxidizer inlet of the injector is usually machined to have a circular hole. The injector used in this study was manufactured with a metal 3D printer but was problematic as the layered metal collapsed when processed into a circular shape. Thus, there is a limit to the angle at which the metal can be layered during additive manufacturing, and accordingly, the oxidizer inlet was designed to have a trapezoidal shape as shown in Fig. 1. The designed injectors target the same operating conditions, and the injection pressure drop must be the same for all injectors. When the oxidizer inlet has the same area, the swirl injector has a higher injection pressure drop than the shear injector, so the oxidizer inlet area of the swirl injector is

designed to be slightly larger. Except for the location/area of the oxidizer inlet and the presence of the fuel injector swirler, the internal geometric parameters that can affect the performance of the coaxial injectors were identical for all injectors. The geometric parameters of the injectors used are summarized in Table 1.

Table 1 Geometric parameters of the injectors

Parameter	Value	Unit
A_h for Inj #A, #B	5.6	mm ²
A_h for Inj #C, #D, #E	7.0	mm ²
n	2	
d_F	6.8	mm
d_O	4.9	mm
L_R	5.5	mm
R	1.1	mm
t_o	0.3	mm
2α	7	°

2.2 Experimental Apparatus

Figure 3 shows the schematic diagram of the experimental apparatus used in this study. Water and air replaced the actual propellant liquid oxygen and gaseous methane as simulated fluids, and a cold flow test was performed at atmospheric pressure. The mass flow rates of water and air were controlled independently. For air, constant pressure was maintained using a high-pressure air tank and a regulator, and the flow rate was controlled through a needle valve and a mass flow meter (Bronkhorst, M15-AAD-22-O-S, uncertainty $\pm 0.5\%$). For water, the water tank was pressurized to a constant pressure using a high-pressure air tank and a regulator, and the set flow rate was supplied using a needle valve and a mass flow meter (Kometer, KMS-2000, uncertainty $\pm 0.15\%$) like air. Moreover, a $90 \mu\text{m}$ filter was installed in front of the needle valve of each simulated propellant to filter out foreign substances.

The injection image was taken with a high-speed camera (Vision Research, Phantom v9.1) and a xenon light source (Polarion, PS-NP1) facing each other with the injection in the middle, with $2 \mu\text{s}$ of exposure and 1 kHz of the sampling rate. Two hundred images were captured for each

experimental condition, and the obtained instantaneous image and the time-averaged image were used to analyze the breakup length and the spray angle.

Figure 4 illustrates the metering sensor connected to the injector manifold. K-type thermocouples (Sentech, uncertainty ± 1.5 K) and pressure transducers (Sensys, PSH-15B/5B, uncertainty $\pm 0.15\%$) were installed at each manifold by branching the liquid oxidant manifold and gaseous fuel supply line. Accordingly, the simulated propellant's temperature and pressure were measured at the injector's front end. The measured temperature, pressure, and mass flow rate data were stored for 1 second for each experimental condition at a sampling rate of 1 kHz through NI-cDAQ (National Instruments™, Compact DAQ system, NI USB-6218). These data were then used to analyze the fluid density in the injector, injection pressure drop, and discharge coefficient.

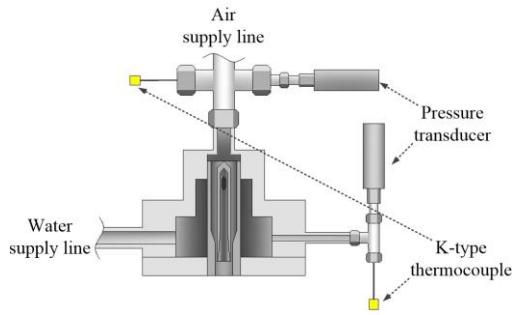


Fig. 4. Schematic of the injector manifolds and installed measurement sensors.

2.3 Experimental Conditions

The injector was designed to be applied to a 3-ton class methane engine. The design pressure of the combustion chamber is 73.5 bar, the oxidizer/fuel mixture ratio is 3.0, and the flow rate conditions of a single injector are 268.0 g/s for liquid oxygen and 89.3 g/s for gaseous methane. The predicted velocity of each propellant at the injector outlet is 12.3 m/s for liquid oxygen and 118.1 m/s for gaseous methane. In this cold flow test, the nominal flow rate was set so that the speed of water and air was identical to that of the actual propellant. Therefore, the nominal flow calculated considering the density ratio of each propellant is 230.94 g/s for water and 1.85 g/s for air. The experiment was carried out under the conditions of a single-injection condition that injected water and air independently and a bi-injection condition that injected water and air simultaneously. Table 2 summarizes the nominal flow rate and each cold flow test's experimental condition.

For a single-injection experiment, water was increased from 10% to 110% in a 10% increment, and the air was increased from 50% to 110% in a 10% increment based on the nominal flow rate. The atomization of the propellant in coaxial injectors is known to depend on the momentum flux ratio between gas/liquid propellant (Woodward *et al.* 2006). The momentum flux ratio is calculated using

Table 2 Nominal and experimental conditions

Design nominal condition	
\dot{m}_{ld} [g/s]	230.94
\dot{m}_{gd} [g/s]	1.85
Experimental conditions under single-injection	
\dot{m}_l / \dot{m}_{ld} [%]	10 ~ 110, $\Delta 10$
\dot{m}_g / \dot{m}_{gd} [%]	50 ~ 110, $\Delta 10$
Experimental conditions under bi-injection	
\dot{m}_l / \dot{m}_{ld} [%]	40
J	1.0 ~ 6.0, $\Delta 1.0$

Eq. (3), and the bi-injection experiment conditions were set accordingly.

$$J = \frac{\rho_g V_g^2}{\rho_l V_l^2} \quad (3)$$

Here, the velocity used in the calculation is axial velocity. For Inj #A and #B, where the liquid oxidizer only has the axial velocity, it can be simply calculated from Eq. (4), but the tangential velocity and the thickness of the liquid film must be considered for Inj #C, #D, and #E.

$$V_l = \frac{4\dot{m}_l}{\rho_l d_o^2} \quad (4)$$

Thus, the thickness of the liquid film according to the flow rate and the injection pressure drop was calculated using Eq. (5), an empirical equation of the open-type swirl-injector proposed by Fu *et al.* (2011). Eq. (6) was used to calculate the axial velocity at the injector outlet (Lee *et al.* 2019).

$$h_l = 3.1 \left(\frac{d_o \dot{m}_l \mu_l}{\rho_l \Delta P_l} \right)^{0.25} \quad (5)$$

$$\dot{m}_l = \rho_l h_l \pi (d_o - h_l) V_l \quad (6)$$

Owing to the nature of the atmospheric pressure cold flow test, there is a limit to increasing the airflow rate to match the momentum flux ratio when the water flow rate is high. Consequently, the water flow rate was fixed at 40% of the nominal flow rate, and the momentum flux ratio was adjusted from 1.0 to 6.0 in a 1.0 increment by increasing the airflow rate.

3. EXPERIMENT RESULTS

3.1 Single-Injection

Fig. 5 illustrates the injection pressure drop against the flow rate under single-injection conditions. The injection pressure drop measured at the oxidizer and fuel injectors tended to be proportional to the square of the mass flow rate, as the theoretical relationship between the mass flow rate and the injection pressure drop. Furthermore, it is confirmed that there is no significant difference in the injection pressure drop for each injector. All injectors were designed with the exact requirements and fabricated through additive layer manufacturing, and the

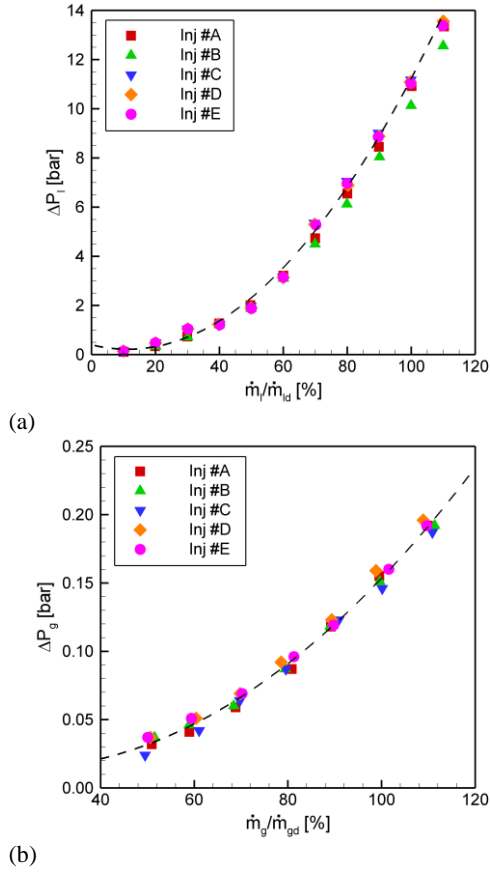


Fig. 5. Injection pressure drop under single-injection through the injector: (a) liquid side and (b) gas side.

injection pressure drop result shows that the application of the additive layer manufacturing for injector production is feasible. For the fuel injector, the presence of a swirler had almost no effect on the injection pressure drop. Under nominal flow rate experimental conditions, the injection pressure drop averaged 10.87 bar water and 0.15 bar air. Calculations considering the density ratio between the simulated propellant and the actual propellant give 12.61 bar liquid oxygen and 7.44 bar gaseous methane, and a similar injection pressure drop is expected during the combustion test.

The discharge coefficient of the injector was calculated using pressure and mass flow rate data under each experimental condition. The liquid discharge coefficient is the ratio of the measured mass flow rate to the theoretically calculated mass flow rate, defined as Eq. (7). The gas discharge coefficient was calculated using Eq. (8) and (9) with compressible fluid flow in consideration (Van den Bosch and Weterings 2005).

$$Cd_l = \frac{\dot{m}_l}{A_o \sqrt{2\rho_l \Delta P_l}} \quad (7)$$

$$Cd_g = \frac{\dot{m}_g}{A_g \psi \sqrt{\rho_g P_g \gamma \left(\frac{2}{\gamma+1}\right)^{\frac{\gamma-1}{\gamma}}}} \quad (8)$$

$$\psi^2 = \frac{2}{\gamma-1} \left(\frac{\gamma+1}{2}\right)^{\frac{\gamma+1}{\gamma-1}} \left(\frac{P_{atm}}{P_g}\right)^{\frac{2}{\gamma}} \left[1 - \left(\frac{P_{atm}}{P_g}\right)^{\frac{\gamma-1}{\gamma}}\right] \quad (9)$$

Figure 6 illustrates the discharge coefficient against the flow rate of each simulated propellant. The discharge coefficient of the oxidizer injector slightly increases as the water flow rate increases and decreases after reaching the peak. This is consistent with the observed characteristics as flow changes into laminar, transitional, and turbulent regions with increasing water flow (Lefebvre and McDonell 2017). Since Inj #C, #D, and #E inject water while spinning tangentially, a gas core is created at the center of the orifice because of the centrifugal force (Ahn and Choi 2017). When $\dot{m}_l/\dot{m}_{ld} \leq 30\%$, the discharge coefficients of Inj #C, #D, and #E were lower than those of Inj #A and #B. This is considered attributable to the centrifugal force not being strong enough, so the gas core was formed incompletely, which can be seen in the spray image in the next section. As the airflow rate increases, the fuel injector discharge coefficient tends to decrease. When $\dot{m}_g/\dot{m}_{gd} \leq 60\%$, the discharge coefficient was slightly higher in Inj #A and #C without swirler, and the discharge rate of all injectors was almost the same when $\dot{m}_l/\dot{m}_{ld} \geq 70\%$. At the same flow rate, the injection pressure drop is higher with than without swirler; but as the flow rate increases, this effect reduces.

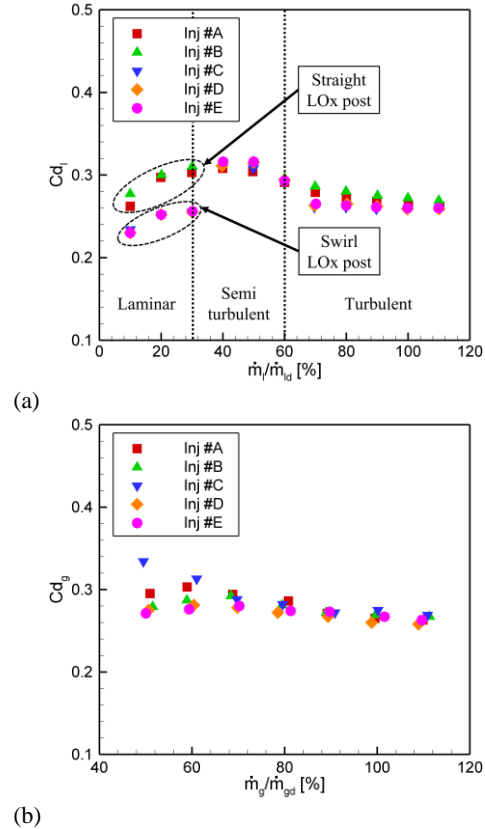


Fig. 6. Discharge coefficient under single-injection through the injector: (a) liquid side and (b) gas side.

3.2 Bi-injection

Figure 7 illustrates the injection pressure drop of the oxidizer and the fuel injectors against the momentum flux ratio under bi-injection conditions. The mass flow rate of water was fixed at $\dot{m}_l/\dot{m}_{la} = 40\%$, but the oxidant injector's injection pressure drop was confirmed to increase with J .

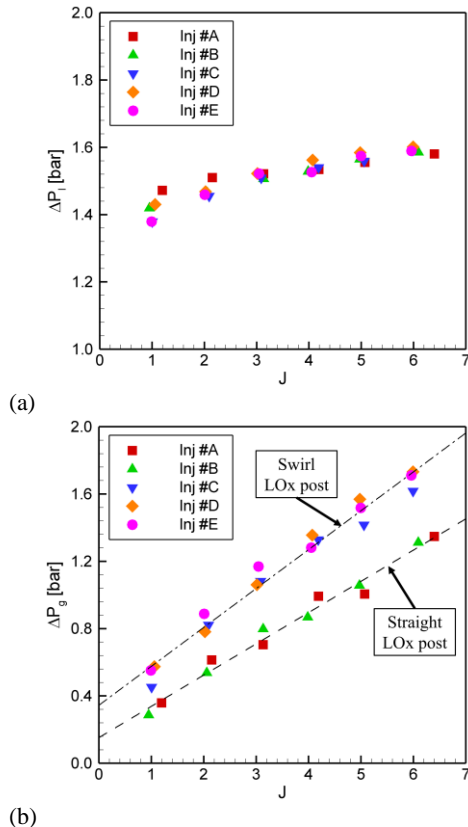


Fig. 7. Injection pressure drop under bi-injection through the injector: (a) liquid side and (b) gas side.

As the momentum flux ratio increases, more air is injected. Therefore, as the gas is injected stronger around the liquid flow in the recess region of the injector, the interference of pushing and influencing the liquid flow toward the center of the injector becomes stronger, thereby increasing the injection differential pressure at the oxidizer post. In the case of an air injection pressure drop, the increase in J represents the increase in the flow rate, and thus the injection pressure drop as a whole increased. Also, Inj #A, B and Inj #C, #D and #E show a difference in tendency. This was because of increased gas flow injection in the case where the oxidizer is injected swirling by the tangential line, the momentum flux ratio was set to equilibrate in the axial direction. Except for these results, there was no difference according to the shape of the fuel post.

Similar to Section 3.1, the discharge coefficient was calculated under each experimental condition, shown in Fig. 8. The difference according to the oxidizer and fuel post shape in the liquid discharge coefficient result was not confirmed like the

injection pressure drop result. Although the mass flow rate of water was the same, the increase in the injection pressure drop affected the flow coefficient results, and the discharge coefficient gradually decreased as J increased. It was confirmed that the gas discharge coefficient increased with the momentum flux ratio.

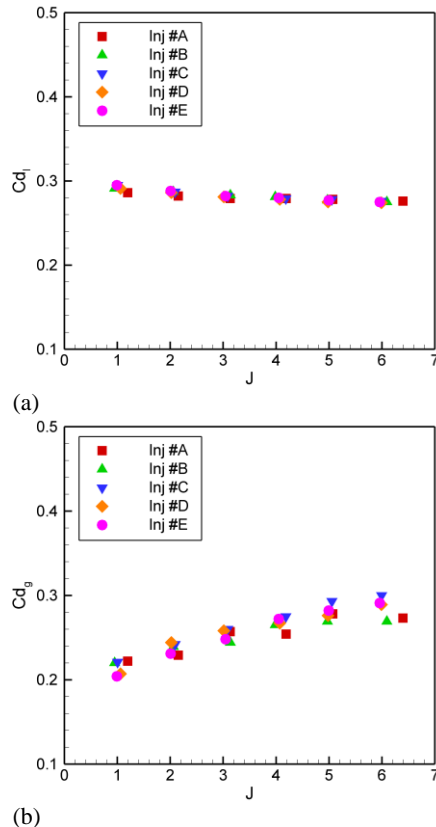


Fig. 8. Discharge coefficient under bi-injection through the injector: (a) liquid side and (b) gas side.

3.3 Image Analysis

Figure 9 shows the instantaneous image results at the time of single-injection captured with a high-speed camera at a sampling rate of 1000 Hz. The results of each injector are shown independently the mass flow rate increases by 20% of the nominal condition toward the bottom of the figure. Depending on the shape of the oxidizer post, the difference in spray shape is clearly identified. In the case of straight oxidizer posts like Inj #A and #B, the liquid core starts to develop in the center of the spray as the liquid flow rate increases, whereas the spray develops in the form of a liquid film in the case of swirl oxidizer posts like Inj #C, #D, and #E. Further, it was confirmed that the injectors with a swirl shape are stable and do not show vibration of the spray with increase in the flow rate, where the injectors with a straight shape were shaken horizontally. This phenomenon occurs because the straight-type injectors have the oxidizer inlet facing toward the center of the injector, where the liquid collides with each other.

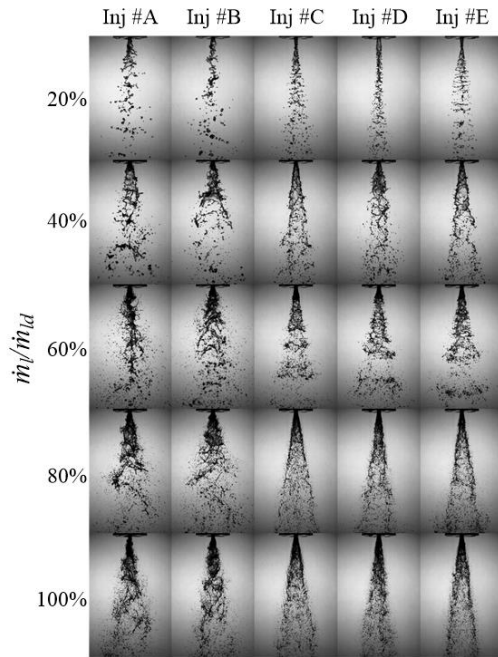


Fig. 9. Instantaneous image of each injector according to the liquid mass flux rate during single-injection.

Figure 10 represents the instantaneous image at the time of bi-injection when J is 1, 3, and 6. As the momentum flux ratio increases, the mixing and atomization on the surface of the spray occur more actively because of the shear force for all injectors, as the relative velocity of the two propellants increases. Also, Inj #A and #B with straight oxidizer post shape had spray gathered at the center than the swirl injector owing to the axial direction of the spray velocity. In contrast, the swirl injector seemed to have a larger spray angle because of the tangential direction of the spray velocity.

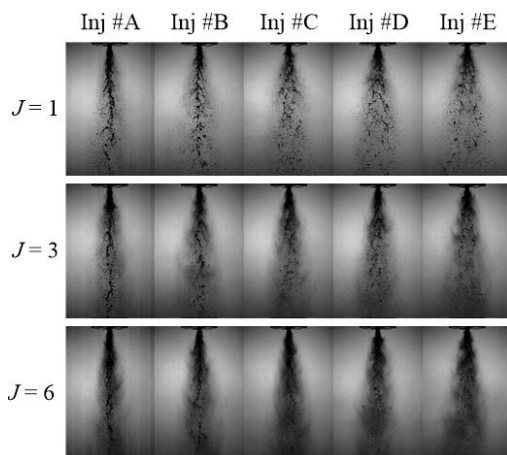


Fig. 10. Instantaneous image of each injector according to the momentum flux ratio during bi-injection.

The breakup length and spray angle were measured to confirm atomization and mixing performance via images captured with a high-speed camera. The

breakup length was determined by binarizing the 200 instantaneous images captured for each experiment condition. The raw spray image is a grayscale image with an intensity of 0-255 per pixel, and a threshold value for binarization was required. Therefore, all images were binarized by selecting a threshold value that minimizes the variance of all binarized pixels (Otsu 1979). Then, the first breakup point was determined in the binarized image, and the vertical length from the injector outlet was defined as the breakup length. Fig. 11 compares the breakup length measured in the instantaneous image and binarized image captured in the $\dot{m}_l/\dot{m}_{td} \leq 30\%$ single-injection experiment. It was confirmed that the breakup length measurement could be performed effortlessly, even in the spray forms that vary depending on the oxidizer post's shape. However, the breakup length tends to measure longer than actual, even when the image is normalized when analyzed similarly in the instantaneous image of bi-injection conditions as seen in Fig. 10 owing to the atomization effect on the spray surface, which causes the image to appear darker. Therefore, the breakup length under bi-injection conditions was analyzed by measuring the vertical length to the breakup point with the visual inspection of 200 images at intervals of 10 for a total of 20 images.

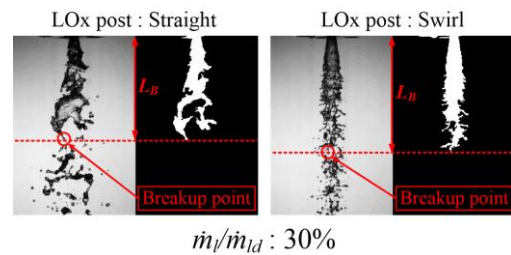


Fig. 11. Determination of breakup length by the instantaneous binarized image.

Figure 12 illustrates the example of a spray angle measurement. Using Otsu's method, the image was binarized as in the breakup length, and the angle was measured from 10 mm point vertical of the injector outlet to the 20 mm point vertical.

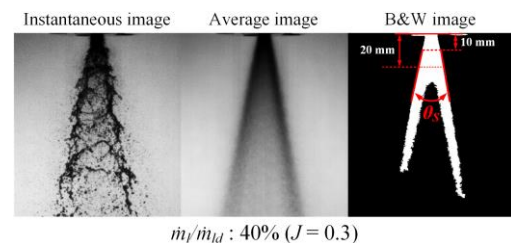


Fig. 12. Determination of spray angle by the averaged binarized image.

Figure 13 represents the measurement of the liquid single-injection experiment's breakup length and spray angle results. In the single-injection experiment, the breakup length and the spray angle showed a difference in the tendency as the flow rate increased based on $\dot{m}_l/\dot{m}_{td} = 50\%$, regardless of the injector. The spray angle develops when the flow

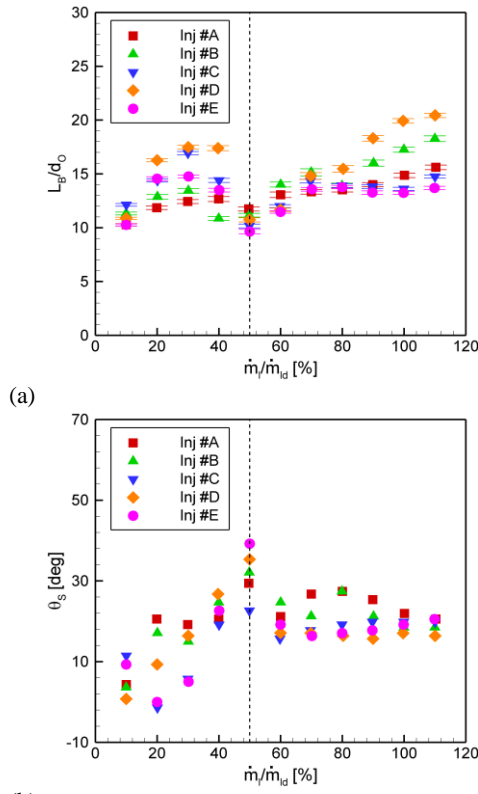


Fig. 13. Results according to the liquid mass flow rate under single-injection: (a) breakup length and (b) spray angle.

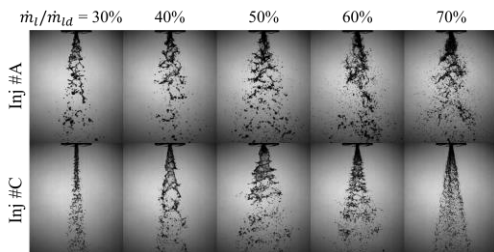


Fig. 14. Instantaneous spray image for mass flow rate and post shape under single-injection.

rate increases up to $\dot{m}_l/\dot{m}_{id} = 50\%$, but when the flow rate increases beyond that point, the spray angle is maintained, and the breakup length gradually increases. Fig. 14 illustrates the instantaneous image result of the injectors with different oxidizer post shapes under $\dot{m}_l/\dot{m}_{id} = 30\% \sim 70\%$ experimental condition. The spray angle development can be observed according to the flow rate increase/decrease based on the $\dot{m}_l/\dot{m}_{id} = 50\%$ condition. The spray angle is not large when the flow rate exceeds 50%, especially when the oxidizer post shape is a swirl.

Figure 15 represents the breakup length and spray angle measurement under bi-injection conditions. In contrast to the single-injection condition where no consistent difference was observed between the injector's different internal structure, there was a consistent difference in the bi-injection condition between different post shapes. This is because they

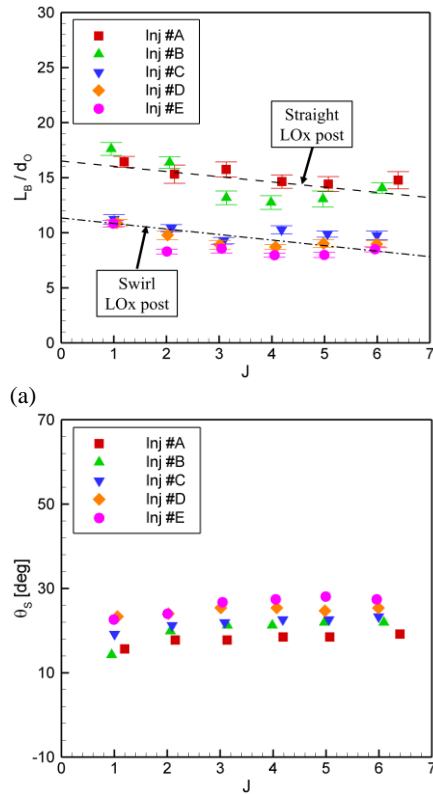


Fig. 15. Results according to the momentum flux ratio under bi-injection: (a) breakup length and (b) spray angle.

have a tangential velocity, and liquid injecting Inj #C, #D, and #E sprays tend to interact with gas relatively more than Inj #A and #B. As a result, the atomization and mixing performance improved, where the breakup length decreased, and the spray angle increased. Although less effective than the shape of the oxidizer post, a difference according to the shape of the fuel post was also confirmed. For the injector with a straight oxidizer post shape, the breakup length was smaller, and the spray angle was larger with Inj #B, which has a swirl-shaped fuel post. For the injector with the swirl oxidizer post shape, the atomization and mixing performance improved in the order of rotating in the same direction (Inj #E), rotating in the opposite direction (Inj #D), and spraying in the axial direction (Inj #C). When the gas rotates while spraying, there are relatively more interactions than spraying in the axial direction. However, when the gas rotates in the opposite direction to the liquid (Inj #D), the rotational momentum of the spray is canceled, lowering the spray angle and adversely affecting the mixing performance of the injector, compared to Inj #E.

The breakup length can judge the atomization performance of the injector and is heavily affected by the velocity of the propellant. Accordingly, many studies have been conducted to confirm the relationship with variables such as Reynolds number, Weber number, momentum flux ratio, and more (Forstall and Shapiro 1950; Au and Ko 1987;

Eroglu *et al.* 1991; Villermaux *et al.* 1994; Engelbert *et al.* 1995; Carreau *et al.* 1997). Among them, the momentum flux ratio is considered to have the greatest influence on the breakup of the liquid injected from the coaxial injector, which was focused on in this study, so as to identify the relationship.

Figure 16 shows the result of the breakup length against the momentum flux ratio, with the results of previous studies that confirmed the relationship between the momentum flux ratio and the breakup length of shear coaxial injectors (Villermaux 1998; Davis *et al.* 2005; Leyva *et al.* 2007). The solid line in Fig. 16 represents the nonlinear fitting equation for each injector. Inj #A and #B, in which the liquid has only axial velocity, were confirmed to coincide with the shear coaxial type breakup length results in terms of their tendency. Whereas the result of Inj #C, #D, and #E shows a shorter breakup length overall, but is confirmed that the slope of the breakup length is consistent with the shear coaxial injectors when momentum flux ratio increases, despite it being a swirl injector. Such a result can be explained by the characteristic of the swirl coaxial injector, which is confirmed as the momentum flux ratio increases. According to Strakey *et al.* (2001) and Jeong *et al.* (2005), the macroscopic characteristic of the swirl and shear coaxial injectors coincides as the momentum flux ratio increases. Therefore, it is confirmed that the breakup length tendency, a macroscopic characteristic of both injector types, becomes almost the same in this study, where the experimental condition was a momentum flux ratio of 1 or higher.

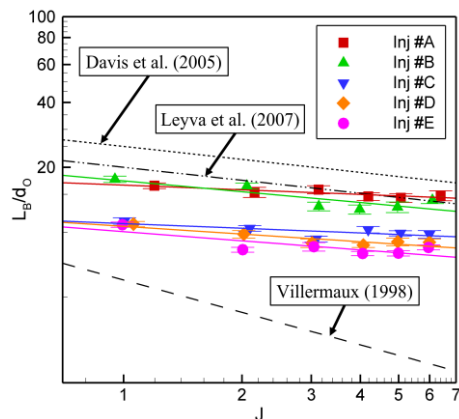


Fig. 16. Breakup length results according to the momentum flux ratio; Villermaux (1998): $L_B/d_o = 6/J^{0.5}$, Davis *et al.* (2005): $L_B/d_o = 25/J^{0.2}$, Leyva *et al.* (2007): $L_B/d_o = 20/J^{0.2}$.

4. CONCLUSION

A total of five types of coaxial injectors were fabricated using the SLM method according to the shape of the oxidizer and fuel post. Cold flow tests were conducted using water and air as simulated propellants under an atmospheric pressure environment. The nominal flow was set based on the expected actual propellant velocity to simulate

the environment inside the combustion chamber. The basic requirements of the injector, including the injection pressure drop and discharge coefficient, were examined, and the breakup length and spray angle were measured using the instantaneous and average images captured by a high-speed camera.

Under the single-injection condition, there was a difference depending on the shape of the oxidizer post. The swirl shape showed a higher injection pressure drop and lower discharge coefficient than the straight shape. Similarly, in the result of the fixed liquid flow rate bi-injection condition, a difference in the tendency according to the oxidizer post shape was confirmed when the flow rate of the gas is increased according to the momentum flux ratio. However, the difference according to the fuel post shape was not clear.

When the breakup length and spray angle were analyzed, no differences were confirmed under single-injection conditions. In contrast, the effect of different oxidizers and fuel post shapes under bi-injection conditions was confirmed. The swirl shape of the oxidizer and the fuel post increased the interaction between the two propellants, confirming the decrease in the breakup length and increase in the spray angle as a result. Furthermore, when the oxidizer and the fuel rotate in opposite directions, the breakup length increases owing to the rotation of the gas, which cancels the liquid momentum, thus lowering the spray angle.

This study investigated how the internal structure of an injector can affect atomization and mixing performance using injectors manufactured by a metal 3D printer. The injectors manufactured by a 3D printer has the disadvantage of having a relatively rougher surface than the metal machined injectors, which was expected to be problematic in the real rocket application. However, there were no significant problems limiting propellant injection and droplet breakup. Accordingly, as confirmed in some experimental conditions, the injector that structurally resolved unstable injection under the straight oxidizer post shape was manufactured in the same way by the SLM method. Finally, the cold flow test and combustion tests are being conducted, and the results will be submitted in a follow-up study.

ACKNOWLEDGEMENTS

This research was supported by the National Research Foundation (NRF-2021M1A3B807772, NRF-2021M1A3B9095872) and the Korea Aerospace Research Institute (KARI-FR21C00) funded by the Ministry of Science, ICT, and Future Planning, South Korea. The authors would like to thank MSIP and KARI for their support.

REFERENCES

Ahn, K. and H. Choi (2017). A study on discharge coefficients of closed-type swirl injectors for a liquid rocket engine. *Atomization and Spray* 27(7), 569-578.

- Atyam, D. M. and P. E. Sojka (2017, July). Characterization of direct metal laser sintered impinging injectors: like doublet, unlike triplet, like quadlet, unlike pentad. In *53rd AIAA/SAE/ASEE Joint Propulsion Conference*, Atlanta, USA.
- Au, H. and N. W. M. Ko (1987). Coaxial jets of different mean velocity ratios, part 2. *Journal of Sound and Vibration* 116(3), 427-443.
- Beer, J. M. and N. A. Chigier (1972). *Combustion Aerodynamics*. Applied Science, London, UK.
- Carreau, J. L., E. Porcheron, D. Le Visage, L. Prevost and F. Roger (1997). Liquid core characterization of coaxial liquid oxygen/inert gas jets. *International Journal of Fluid Mechanics Research* 24(4-6), 498-507.
- Cohn, R. K., P. A. Strakey, R. W. Bates and D. G. Talley (2003, January). Swirl coaxial injector development. In *41st Aerospace Sciences Meeting and Exhibit*, Reno, USA.
- Davis, D., B. Cherroudi and D. Talley (2005, December). Experiments on a coaxial injector under an externally-forced transverse acoustic field. In *53rd JANNAF Joint Propulsion Meeting, 2nd Liquid Propulsion, 1st Spacecraft Propulsion Subcommittee*, Monterey, USA.
- Engelbert, C., Y. Hardalupas and J. Whitelaw (1995). Breakup phenomena in coaxial airblast atomizers. *Proceeding of the Royal Society of London, Series A: Mathematical Physical Sciences* 451(1941), 189-229.
- Eroglu, H., N. Chigier and Z. Farago (1991). Coaxial atomizer liquid intact lengths. *Physical of Fluids A* 3(2), 303-308.
- Forstall, Jr, W. and A. Shapiro (1950). Momentum and mass transfer in coaxial gas jets. *Journal of Applied Mechanics* 17(4), 399-408.
- Fu, Q., L. Yang and Y. Qu (2011). Measurement of annular liquid film thickness in an open-end swirl injector. *Aerospace Science and Technology* 15, 117-124.
- Glogowski, M. and M. Micci (1995, July). Shear coaxial injector spray characterization near the post tip region. In *31st AIAA/ASME/SAE/ASEE Joint Propulsion Conference and Exhibit*, San Diego, USA.
- Howell, E. (2014). SpaceX Taking 3D Printing to the Final Frontier. <https://www.space.com/26899-spacex-3d-printing-rocket-engines.html>
- Huzel, D. K. and D. H. Huang (1992). *Modern engineering for design of liquid-propellant rocket engines*. Progress in Astronautics and Aeronautics, Washington, D. C., USA.
- Jeong, W. H., D. Kim, J. H. Im and Y. Yun (2005). A study on characteristics of gas/liquid coaxial sprays under varying flow conditions. *Journal of the Korean Society for Aeronautical and Space Sciences* 33(1), 54-61.
- Lee, K. O., B. Lim, D. J. Kim, M. Hong and K. Lee (2020). Technology trends in additively manufactured small rocket engines for launcher applications. *Journal of the Korean Society of Propulsion Engineers* 24(2), 73-82.
- Lee, W., D. Hwang, K. Ahn and Y. Yoon (2019). Spray characteristics of effervescent swirl injectors for variable thrust. *Journal of the Korean Society of Propulsion Engineers* 23(2), 1-12.
- Lefebvre, A. H. and V. G. McDonell (2017). *Atomization and Sprays*. CRC Press Taylor & Francis Group, Boca Raton, USA.
- Leyva, I. A., B. Cherroudi and D. Talley (2007, July). Dark core analysis of coaxial injectors at sub-, near-, and supercritical pressure in a transverse acoustic field. In *43rd AIAA/ASME/SAE/ASEE Joint Propulsion Conference and Exhibit*, Cincinnati, USA.
- Lim, H. Y. and W. R. Roh (2019, November). Selective laser melting (SLM) for LOx/Methane mixing head. In *53rd KSPE Fall Conference*, Busan, Korea.
- Otsu, N. (1979). A threshold selection method from gray-level histograms. *IEEE Transactions on Systems, Man, and Cybernetics* 9(1), 62-66.
- Relativity Space* (2020). Terran 1 Technical Specifications. <https://www.relativityspace.com/terran>
- Soller, S., A. Barata, S. Beyer, A. Dahlhaus, D. Guichard, E. Humbert, J. Kretschmer and W. zeiss (2016, May). Selective laser melting (SLM) of inconel 718 and stainless steel injectors for liquid rocket engines. In *5th Space Propulsion Conference*, Roma, Italy.
- Soller, S., R. Behr, S. Beyer, F. Laithier, M. Lehmann, A. Preuss and R. Salapete (2017, July). Design and testing of liquid propellant injectors for additive manufacturing. In *7th European Conference for Aerospace Science*, Milan, Italy.
- Soller, S., S. Beyer, A. Dahlhaus, A. Konrad, J. Kretschmer, N. Rackemann and W. Zeiss (2015, June-July). Development of liquid rocket engine injectors using additive manufacturing. In *6th European Conference for Aerospace Science*, Kraków, Poland.
- Strakey, P. A., D. G. Talley and J. J. Hutt (2001). Mixing characteristics of coaxial injectors at high gas/liquid momentum ratios. *Journal of Propulsion and Power* 17(2), 402-410.
- Terracciano, A., S. Carapellese, G. Bianchi, D. Liuzzi, M. Rudnykh, D. Drigo and F. Del Brusco (2017, July). Additive layer manufacturing technology in avio injector head design. In *7th European Conference for Aerospace Science*, Milan, Italy.
- Van den Bosch, C. J. H. and R. A. P. M. Weterings (2005). *Methods for the calculation of physical*

- effects (Yellow Book)*. CPR 14E, The Hague, Netherlands.
- Villermaux, E. (1998). Mixing and spray formation in coaxial jets. *Journal of Propulsion and Power* 14(5), 807-817.
- Villermaux, E., H. Rehab and E. Hopfinger (1994). Breakup régims and self-sustained pulsations in coaxial jets. *Meccanica* 29(4), 393-401.
- Woodward, R. D., S. Pal, S. Farhangi and R. J. Santoro (2006, July). LOX/GH₂ shear coaxial atomization studies at large momentum flux ratios. In *42nd AIAA/ASME/SAE/ASEE Joint Propulsion Conference & Exhibit*, Sacramento, USA.
- Yap, C. Y., C. K. Chua, Z. L. Dong, Z. H. Liu, D. Q. Zhang, L. E. Loh, and S. L. Sing (2015). Review of selective laser melting: materials and applications. *Applied Physics Reviews* 2(4), 041101.